Dentomaxillofacial Radiology (2017) 46, 20160225

birpublications.org/dmfr

RESEARCH ARTICLE

An automatic panoramic image reconstruction scheme from dental computed tomography images

[1]Thekla K Papakosta, [1]Antonis D Savva, [1]Theodore L Economopoulos, [1]George K Matsopoulos and [2]H G Gröhndal

[1]School of Electrical and Computer Engineering, National Technical University of Athens, Athens, Greece; [2]Department of Oral and Maxillofacial Radiology, Institute of Odontology, University of Gothenburg, Gothenburg, Sweden

Objectives: Panoramic images of the jaws are extensively used for dental examinations and/or surgical planning because they provide a general overview of the patient's maxillary and mandibular regions. Panoramic images are two-dimensional projections of three-dimensional (3D) objects. Therefore, it should be possible to reconstruct them from 3D radiographic representations of the jaws, produced by CBCT scanning, obviating the need for additional exposure to X-rays, should there be a need of panoramic views. The aim of this article is to present an automated method for reconstructing panoramic dental images from CBCT data.
Methods: The proposed methodology consists of a series of sequential processing stages for detecting a fitting dental arch which is used for projecting the 3D information of the CBCT data to the two-dimensional plane of the panoramic image. The detection is based on a template polynomial which is constructed from a training data set.
Results: A total of 42 CBCT data sets of real clinical pre-operative and post-operative representations from 21 patients were used. Eight data sets were used for training the system and the rest for testing.
Conclusions: The proposed methodology was successfully applied to CBCT data sets, producing corresponding panoramic images, suitable for examining pre-operatively and post-operatively the patients' maxillary and mandibular regions.
Dentomaxillofacial Radiology (2017) **46**, 20160225. doi: 10.1259/dmfr.20160225

Cite this article as: Papakosta TK, Savva AD, Economopoulos TL, Matsopoulos GK, Gröhndal HG. An automatic panoramic image reconstruction scheme from dental computed tomography images. *Dentomaxillofac Radiol* 2017; **46**: 20160225.

Keywords: dental X-ray panoramic images; Cone beam computed tomography; image processing; image reconstruction; pre-operative and post-operative maxilla assessment

Introduction

CBCT images are commonly used in dental applications from treatment planning to the monitoring of the progression or regression of bony lesions.[1,2] Commonly, CBCT images depict the full three-dimensional (3D) anatomy of the examined region. Nevertheless, they do not provide an overview of the region as provided by a panoramic image. A panoramic view can be acquired either by exposing the patient to an additional amount of radiation or through a curved multiplanar reconstruction, in which case the curve of the jaw in an axial CBCT slice has to be annotated manually.[3,4] Alternatively, panoramic images can be reconstructed from the 3D CBCT volumes by means of a semi-automated or fully automated process.

The primary process of the reconstruction is the detection of an appropriate dental arch from one of the CT slices. Then, the dental arch is isolated and the reconstructed panoramic image is formed by considering the projection of the detected dental arch in preceding and subsequent CT slices. This approach was

Correspondence to: Prof. George Konstantinos Matsopoulos. E-mail: gmatso@esd.ece.ntua.gr
Received 26 May 2016; revised 21 December 2016; accepted 11 January 2017

adopted by several researchers, leading to the introduction of numerous semi-automatic or fully automatic panoramic reconstruction techniques.[5–10]

Thali et al[5] proposed a non-automatic method to draw the dental arch and to reconstruct the panoramic image for post-mortem identification purposes. In the particular study, a software package (DentaScan; General Electric Healthcare, Aurora OH) was used, allowing the reconstruction of images similar to conventional panoramic views, by manually defining the slice containing the dental arch.[6] This methodology can be used to build multiple panoramic and cross-sectional views from axial CT data sets. More significantly, this method requires a fair amount of user intervention (from the clinical expert/doctor) to extract the final panoramic dental image. In addition, the particular method cannot deal with cases where metallic implants are present, causing distorted panoramic images.[5]

Towards a procedure with minimal human intervention, Chanwimaluang et al[7] proposed an algorithm that automatically detects the dental arch in a given axial CT slice. This technique consists of multiple processing stages for initially detecting the dental arch which is then used to reconstruct the panoramic image. Firstly, a local entropy thresholding technique is implemented to isolate the region of interest of the two-dimensional (2D) CT slice containing the dental arch.[7,11] Then, the resulting binary image is fed into the subsequent processing steps: connected component labelling, morphological dilation, thinning and curve fitting to detect the dental arch.[7] Finally, the panoramic images are generated based on the results derived from the previous procedure. Even though the particular method is considered to be an automatic technique, it lacks accuracy in terms of detecting the dental arch when individual teeth or larger bony structures are missing.[7]

The method proposed by Bing et al[8] attempts to address the aforementioned drawbacks. In the particular technique, the dental arch is obtained by computing the maximum intensity projection of the horizontal CT slices. Then, after a series of morphological operations, a reference curve is obtained, on which the dental arch detection is based. Finally, the panoramic images are generated and reconstructed. Despite the fact that this method is considered as fully automatic, the quality of the obtained results highly depends on several internal parameters of the system, which render its performance highly dependent on the processed data.[8]

Vera et al[9] minimized human intervention to the extent of just selecting an appropriate axial CT dental scan. In this case, the subsequent steps include non-linear operations on the chosen CT slice to detect the dental arch, which is estimated using a cubic curve fitting algorithm. Finally, the panoramic images are reconstructed by taking into consideration more than one offset curve as the dental arch. A shortcoming of this technique is the requirement from the clinical expert/doctor to manually select the 2D CT reference image, which will be in turn used for extracting the dental arch as well as the offset curves.[9]

Finally, Akhoondali et al[10] proposed a fully automatic method for detecting the dental arch and reconstructing the panoramic images. This approach requires three distinct steps: mandibular region isolation, mandibular curve creation and panoramic image extraction. In this case, a CT slice containing the dental arch is manually selected based on a maximum intensity projection of the maxilla. Next, this image is processed through a pipeline consisting of a variety of basic image processing procedures to identify the dental arch. Then, spline fitting is used before the reconstruction of the panoramic images. Even though this method is fully automatic, it does not take into consideration metallic artefacts (such as fixation screws or implants) that may hinder the automatic slice selection procedure.[10] Furthermore, this method is unable to deal with cases where teeth or entire perioral regions are missing or are heavily malformed.[10]

Apart from the previously mentioned research works, there are also commercial systems which provide panoramic reconstruction utilities through manual, semi-automatic and fully automatic procedures. In particular, DentaScan is a software tool which facilitates the creation of axial, oblique and panoramic images of the mandible and maxilla from CT scans of the jaw and mouth area through manual definition of the dental arch.[6] Similar functionality is also provided by the SkyView system which provides reconstructions resembling dental panoramic images.[12] Finally, the i-CAT® Tru-Pan™ system seems to implement an automated method for panoramic image reconstruction.[13] However, the particular software can only be used with the provided CBCT scanner hardware.

Considering all of the above, the purpose of this study is to provide a robust, automatic method for reconstructing panoramic images from CBCT 3D volumes, which is independent of the image acquisition hardware. The proposed methodology comprises of several component algorithms for selecting the appropriate CBCT slice, detecting the dental arch and then reconstructing panoramic images that are similar to actual X-ray panoramic radiographs. In particular, the axial CBCT scan is enhanced and binarized to detect the shape of the dental arch. Subsequent processes include various morphological operations to refine the initial selected region of interest and finally perform standard curve fitting for detecting a candidate dental arch. The final dental arch is determined by assessing the similarity of each candidate arch to a template polynomial. The intensities along the detected final dental arch are projected to a 2D plane to generate the required panoramic image. Potentially, the panoramic images created by the proposed technique could be then used to compare the pre-operative and post-operative condition of patients undergoing, for example, bone augmentation surgical treatment.

Methods and materials

The proposed technique examines each slice of the original CBCT data and tries to identify and isolate the dental arch. The panoramic image is produced from a single fitting dental arch which is determined automatically by comparing the individual curves obtained from each CBCT slice to a template polynomial. The methodology was applied to 42 CBCT data sets comprising of pre-operative and post-operative acquisitions from 21 patients.

Data acquisition

21 patients with alveolar defects and requiring implant therapy were treated in a surgical approach consisting of 2 stages.[14] The first stage involved an augmentation surgical procedure, using a partial thickness flap design and the insertion of implants where possible. After 9–12 months, re-entry was performed. At this stage, previously exposed implant surfaces were covered by newly formed hard tissue. Finally, healing abutments were inserted. From the 21 patients, 42 data sets were produced (2 for each patient) from the applied surgical protocol for alveolar ridge augmentation described above. The surgical procedures were performed, and the resulting data sets were provided by the Department of Periodontology, Semmelweis University, Budapest, Hungary.

Each set consists of two volumes of CBCT images from the pre-operative and post-operative examinations of each patient. The CBCT slices in each case comprise a full 3D representation of the patient's jaws focusing on alveolar changes before and after surgery. All data

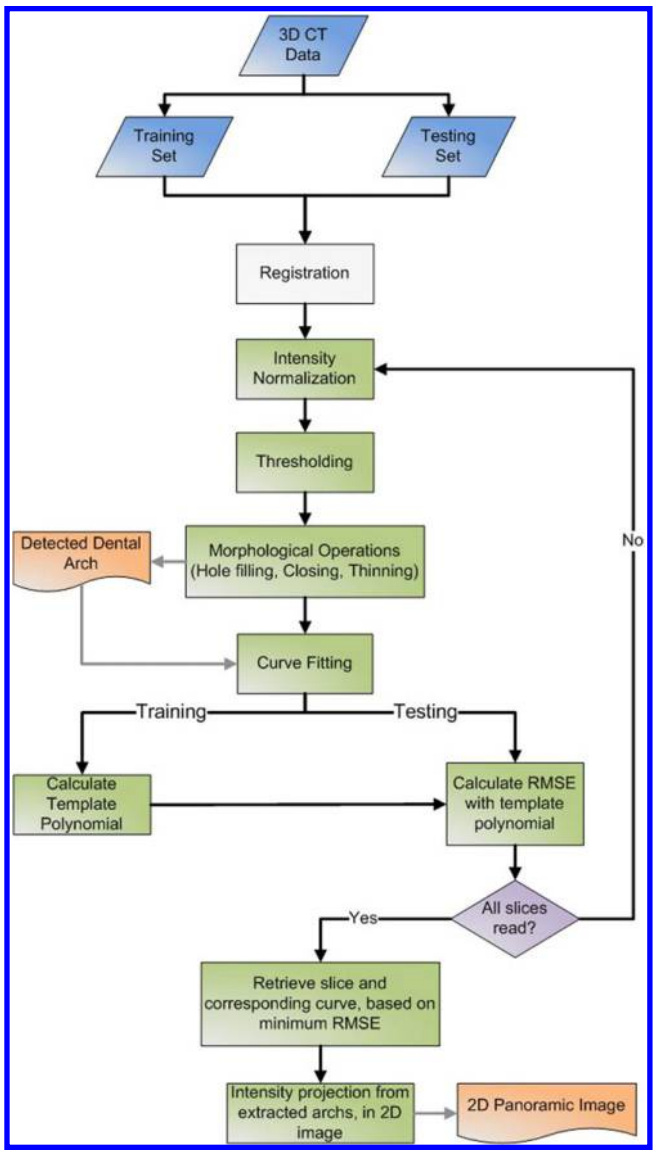

Figure 1 Overview of the proposed methodological scheme for automatic dental panoramic image reconstruction. 2D, two-dimensional; 3D, three-dimensional; RMSE, root mean square error.

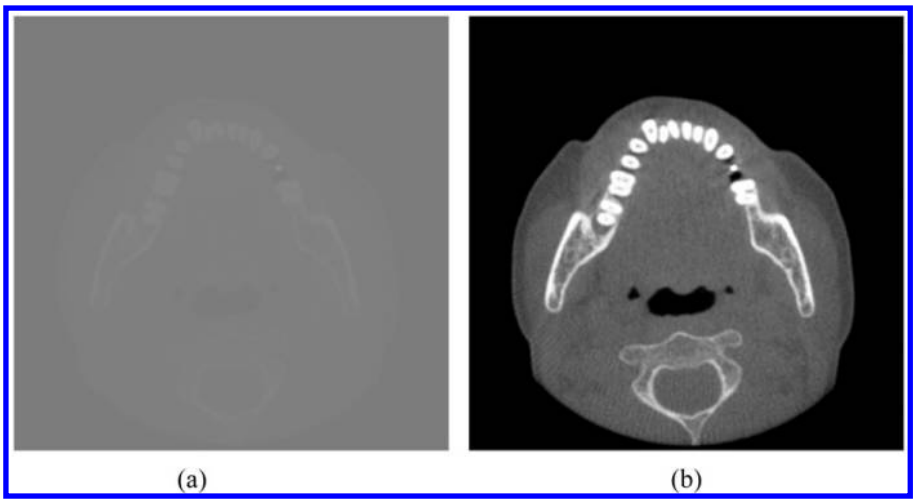

Figure 2 Overview of the effect of intensity normalization: (a) initial image and (b) image after intensity adjustment.

sets were acquired using an i-CAT scanner with the following parameters: high frequency, constant potential, fixed anode 120 kVp, 3–8 mA (pulse mode). The image detector was an amorphous silicon flat panel with a size of 20 × 25 cm. All available data sets are formatted in the digital imaging and communications in medicine (DICOM) standard as a series of 16-bit grey-scale images (corresponding to individual CT slices). The size of all images is 400 × 400 pixels, with a 0.4 × 0.4-mm pixel size. The interslice distance was kept constant for all sets at 0.4 mm. The number of slices (images) in each set was from 322 to 327, depending on the patient. For the needs of the current study, a total of eight data sets were extracted from the initial ones (either pre-operative or post-operative) and considered to be the training set, whereas the remaining 34 were used to test the proposed methodology. Those 34 data sets correspond to 17 patients (pre-operative and post-operative acquisitions), of which 11 were females and 6 males, aged from 39 to 76 years. In addition, the eight data sets used for training correspond to eight patients, one female and seven males, aged from 34 to 77 years.

The selection of the data sets included in the training group was based on the consistency of the detected dental archs. In this case, the considered data sets exhibited the best possible formed dental archs without discontinuities in the bone tissue and without artefacts caused by implants or fixation screws, which was a common case in the available data sets, due to the applied clinical protocol. These sets were selected manually and were validated by collaborating dental experts.

Automatic panoramic reconstruction scheme

The proposed methodological scheme consists of several distinct image-based techniques which are carried out sequentially. An overview of the applied methodology can be seen in Figure 1. The training set is used for deriving a template polynomial, *i.e.* a polynomial which describes the shape and curvature of a typical dental arch. Data from the testing set are used to evaluate the proposed methodological scheme in terms of reconstructing the panoramic images. In both cases (training and testing sets), the same pre-processing pipeline is applied as can be seen in Figure 1 and as described below.

Initially, an optional processing step is applied to align the pre-operative and post-operative CBCT volumes, through an algorithmic procedure called image registration.[14] In this study, registration was applied to the 3D CBCT volumes prior to panoramic reconstruction. The reason for including the aforementioned procedure in the proposed methodology is that the aligned CBCT volumes will result in the

Figure 3 Binary image after automatic threshold calculation.

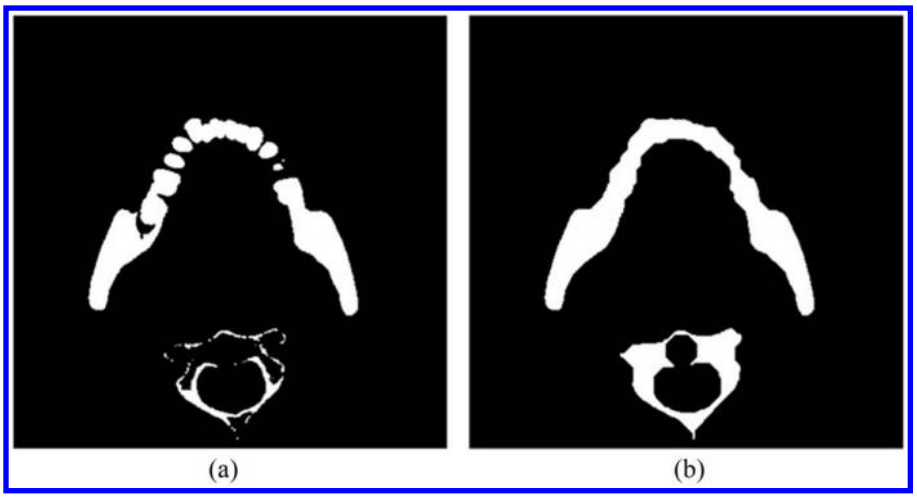

Figure 4 Resulting image after (a) hole filling and (b) morphological closing using a disc of radius 15 pixels as the structuring element.

reconstruction of aligned panoramic images, which can be directly compared and clinically assessed by a medical expert. The employed 3D registration scheme included an affine transformation, together with the Downhill Simplex optimization method and the Mattes mutual information metric for aligning the post-operative data according to the spatial characteristics of the pre-operative data.[14] The usefulness of the particular step is further examined in the Discussion section.

Following the optional registration step, for each data volume, any possible brightness and contrast differences between subsequent CBCT slices are corrected. Then, these images are converted to binary using an automatically calculated threshold. Further basic image processing algorithms are applied on the resulting binary images, such as hole-filling, morphological closing and morphological thinning. This allows the automated detection of a candidate dental arch. For each slice, a candidate dental arch is modelled as a polynomial curve and then compared with the template curve extracted from the training set, in terms of the root mean square error (RMSE). The slice that minimizes the RMSE metric is considered as the one containing the desired dental arch. Once an appropriate dental arch is detected, the intensities of the original CBCT along the arch are projected in a 2D image, thus generating the required dental panoramic image.

Intensity normalization

The individual 2D image slices of the employed 3D CBCT DICOM data volumes need to be pre-processed, as the contrast of the original images is too low. An example of such an image is shown in Figure 2a, where the area of interest cannot be distinguished. Therefore, a correction of the intensity values of each pixel is required. In this study, a simple linear mapping to the interval [0,1] is performed, according to the following equation:

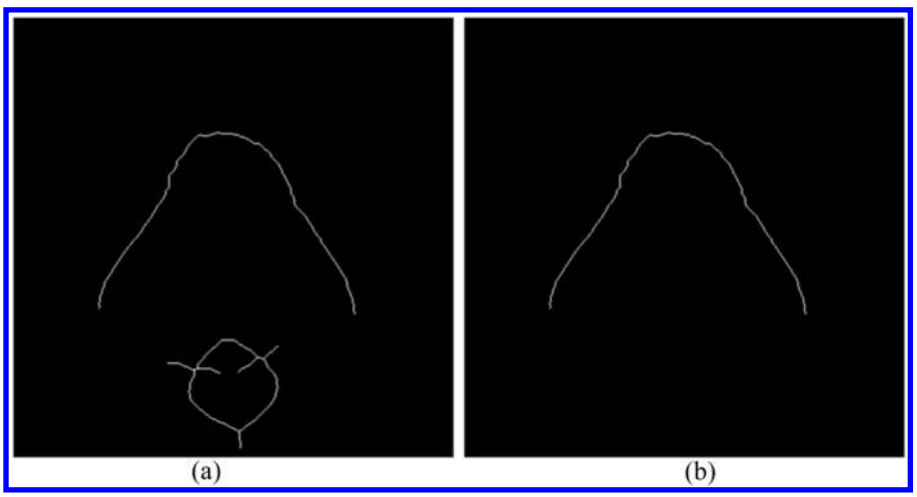

Figure 5 Intermediate resulting images showing (a) morphological thinning and (b) the detected dental arch.

$$I_N(x,y)=(\ I(x,y)-I_{min}\ )\frac{1}{I_{max}-I_{min}} \quad (1)$$

where $I_N(x,y)$ represents each pixel of the new image with the normalized intensity, $I(x,y)$ is the respective pixel of the original image, and I_{min} and I_{max} are the minimum and maximum intensity values of the original image, respectively.

The result of this procedure is illustrated in Figure 2. As can be seen in Figure 2b, the contrast of the image is enhanced relative to the original image (Figure 2a), and therefore the region of interest from which the dental arch will be extracted can be distinguished.

Thresholding

The conversion of the adjusted image to binary form is required for obtaining an initial estimation of the dental arch's position and shape. The objective of this process is to isolate the bright areas which usually represent the teeth and the bony structures. In particular, each pixel of the input image is assigned a value of 1 if its gray level value is above a certain threshold T and 0 if otherwise. Figure 3 shows the resulting binarized image. As can be seen in Figure 3, an initial approximation of the dental arch can be obtained. For the particular data sets used in this study, a different threshold T was used in each case, based on Gaussian fitting of the intensity histogram of the image I_N. In particular, an iterative non-linear least squares fitting approach was employed to calculate an estimate of the two parameters of a Gaussian function, namely the mean value μ and standard deviation σ. Then, the threshold for binarization was set to $T = \mu + w\sigma$, where $w = 3$. The choice of the value of the weighting factor w is further discussed in the Discussion section.

Morphological operations (hole filling, closing, thinning)

The primary objective of this processing step is to eliminate any holes or gaps that may exist in the resulting binary image. Gaps and holes are likely to exist as it is quite common for some patients to have missing teeth or damaged bone tissue. Therefore, through the application of morphological reconstruction operation, the hole filling procedure is implemented to remove possible discontinuities.[15] This step requires the definition of a disc-shaped structuring element with a radius of 15 pixels (6 mm), which was determined after a series of trials. More details regarding the choice of this parameter are mentioned in the Discussion section. After hole filling, a morphological closing filter is applied to refine the results of the previous processing step, as well as for correcting possible discontinuities of the dental arch. The results of these two procedures are presented in Figure 4. Specifically, Figure 4a illustrates the effects of the hole-filling algorithm, whereas Figure 4b shows the results of the morphological closing operation.

After the application of those basic morphological operators, the dental arch is a fully connected region.

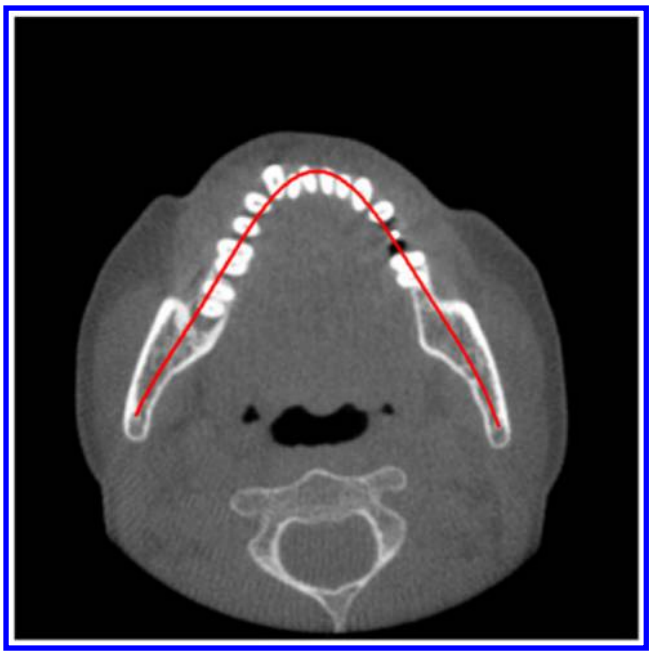

Figure 6 Overlay of the fitted curve on the initial image.

To identify and model the arch using a polynomial, it is essential to apply a morphological thinning operation to the image after the application of the closing operation. Thinning is a morphological operation commonly used for discarding pixels belonging to the foreground to reduce all binary objects to single-pixel thickness.[16–19] Figure 5 shows the effect of the morphological thinning procedure, where all curves have been reduced to a width of a single pixel.

Finally, the arch-shaped curve on which the teeth are situated needs to be isolated. As can be seen in Figure 5a, there are other curves apart from the desired dental arch. In general, the curve corresponding to the dental arch is the longest one. Using this convention, the dental arch can be successfully isolated, as can be seen in Figure 5b. All relevant morphological operations and mathematical background are fully described in Appendix A.

Table 1 Polynomial coefficients (in pixels) of each case in the training set

	Polynomial coefficients						
Case	p_0	p_1	p_2	p_3	p_4	p_5	p_6
#1	63.597	−3.606	161.494	−1.082	−76.510	−0.387	17.020
#2	63.091	3.070	147.406	−5.331	−82.032	2.814	23.358
#3	64.698	−0.903	123.445	−0.585	−38.590	−1.543	7.907
#4	76.725	−4.093	124.395	4.339	−57.703	−1.314	13.813
#5	88.163	−1.304	130.438	1.395	−45.949	−0.194	9.410
#6	117.652	−4.015	120.404	5.025	−36.310	−0.942	7.092
#7	54.048	−0.168	136.143	6.066	−51.372	−3.065	9.740
#8	61.203	0.774	145.577	−2.385	−59.752	1.478	12.334
μ	73.647	−1.281	136.163	0.930	−56.027	−0.394	12.584
σ	20.661	2.545	14.333	3.991	16.598	1.830	5.445
c_v	0.281	−1.987	0.105	4.291	−0.296	−4.643	0.433

The mean (μ), standard deviation (σ) and coefficient of variation (c_v) are also recorded.

Curve fitting
The result of the thinning process can be modelled as a polynomial which is defined by a set of coefficients. In this study, a sixth degree polynomial was used as shown in Equation (2). The selection of the polynomial degree is further discussed in the Discussion section.

$$f(x)=p_6x^6+p_5x^5+p_4x^4+p_3x^3+p_2x^2+p_1x+p_0 \qquad (2)$$

An example of an estimated polynomial is shown in Figure 6, where the polynomial closely matches the dental arch. The aforementioned image-processing techniques result in the representation of the dental arch as a single, continuous curve. The aim of the curve-fitting step is to calculate the corresponding sixth degree polynomial of the dental arch and then to compare it to the template polynomial which is extracted from the training data set.

Template polynomial estimation
To estimate the template polynomial, the following procedure was applied for deriving the polynomial's coefficients. For each of the eight training data sets, the slice which best represented the dental arch was selected. Then, in each one of the selected images, the following processing was applied: (i) intensity normalization, (ii) binarization, (iii) hole filling, (iv) morphological closing, (v) thinning, (vi) curve detection and (vii) curve fitting. All of the aforementioned steps are similar to the ones applied during the processing of the testing set. This procedure resulted in seven polynomial coefficient values for each one of the eight data sets. These values are summarized in Table 1.

Each row of Table 1 presents the calculated values for each data set in the training set, whereas the last rows illustrate the mean value, standard deviation and coefficient of variation ($c_v=\sigma/\mu$) for each polynomial coefficient. The mean values form the template polynomial used in the current study. The relatively high standard deviation and coefficient of variation values are caused by the diversity of the mandibular anatomy of the selected patients. The final template polynomial is illustrated in Equation (3).

$$f(x)=12.584x^6-0.394x^5-56.027x^4+0.930x^3+136.163x^2-1.281x+73.647 \qquad (3)$$

Selection of a fitting dental arch for testing data sets
After the coefficients of the template polynomial have been calculated, they can be compared with the coefficients produced by the curve-fitting procedure previously mentioned. Curve-fitting produces an individual curve for each CBCT slice. From these curves, an appropriate one should be selected for reconstructing the final panoramic image. The similarity between each of those candidate curves and the template polynomial is evaluated, and the most similar curve is selected for panoramic reconstruction. The similarity metric used in this case is the RMSE illustrated in the following equation:

$$\mathrm{RMSE}=\sqrt{\frac{1}{n}\sum_{i=1}^{n}(y_i-\hat{y}_i)^2} \qquad (4)$$

where y_i represent the points of the template polynomial and $\hat{y}_i$ represent the points of the candidate curve. The RMSE value shown in Equation (4) is calculated for each slice of the data. After all slices are processed and all the corresponding RMSE values are calculated, the

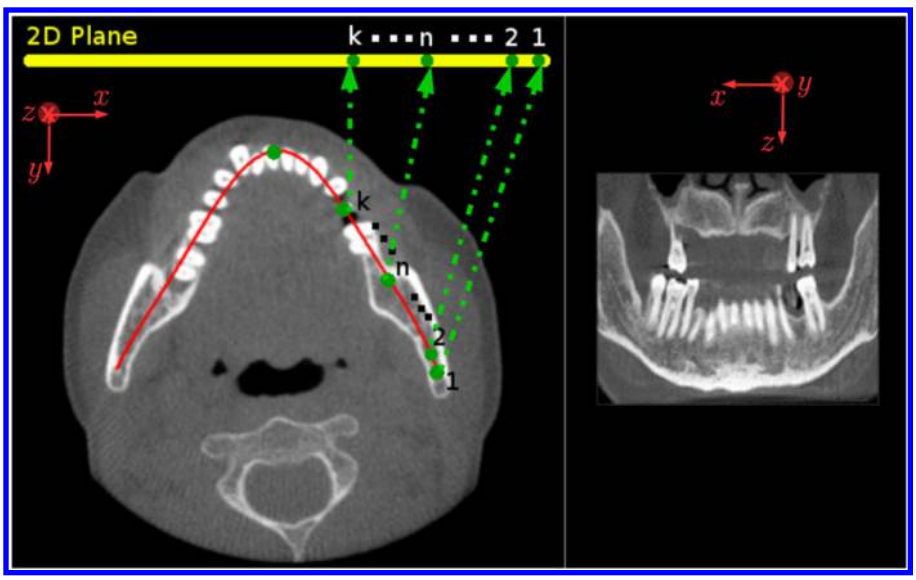

Figure 7 The projection process for reconstructing the final panoramic image, including the corresponding co-ordinate systems (digital imaging and communications in medicine—panoramic view). 2D, two-dimensional.

slice which is associated to the minimum RMSE value is selected for producing the final panoramic image.

Panoramic image

Finally, panoramic image reconstruction is achieved by projecting the intensities of the original CBCT data along the detected dental arch in the plane of a 2D image, thus generating the required dental panoramic image. An illustration of the projection procedure can be seen in Figure 7. To that end, for each CBCT slice, every point along the detected dental arch is serially arranged on the 2D plane, for reconstructing a single line of the panoramic view. The final panoramic image is synthesized after combining all reconstructed lines from all CBCT slices. An example of a final panoramic image is illustrated in Figure 8.

Implementation and testing environment

All of the processing steps featured in this study were implemented in the MATLAB® (MathWorks®, Natick, MA) environment. The implementations were based on the Image Processing Toolbox provided by MathWorks.[20] All tests were performed on a common reference system (Intel® i7 processor at 3.5 GHz, 16 GB of random access memory, running on a 64-bit Linux operating system). In general, the overall processing did not exceed 40 s in any case.

Results

The proposed methodology was applied to CBCT volumes acquired from 17 real clinical cases (34 pre-operative and post-operative data sets). The qualitative results are illustrated in Figure 9, where six representative cases are presented. In each case, the image on the left-hand side indicates the pre-operative case, whereas the image on the right-hand side showcases the post-

Figure 8 Final panoramic image.

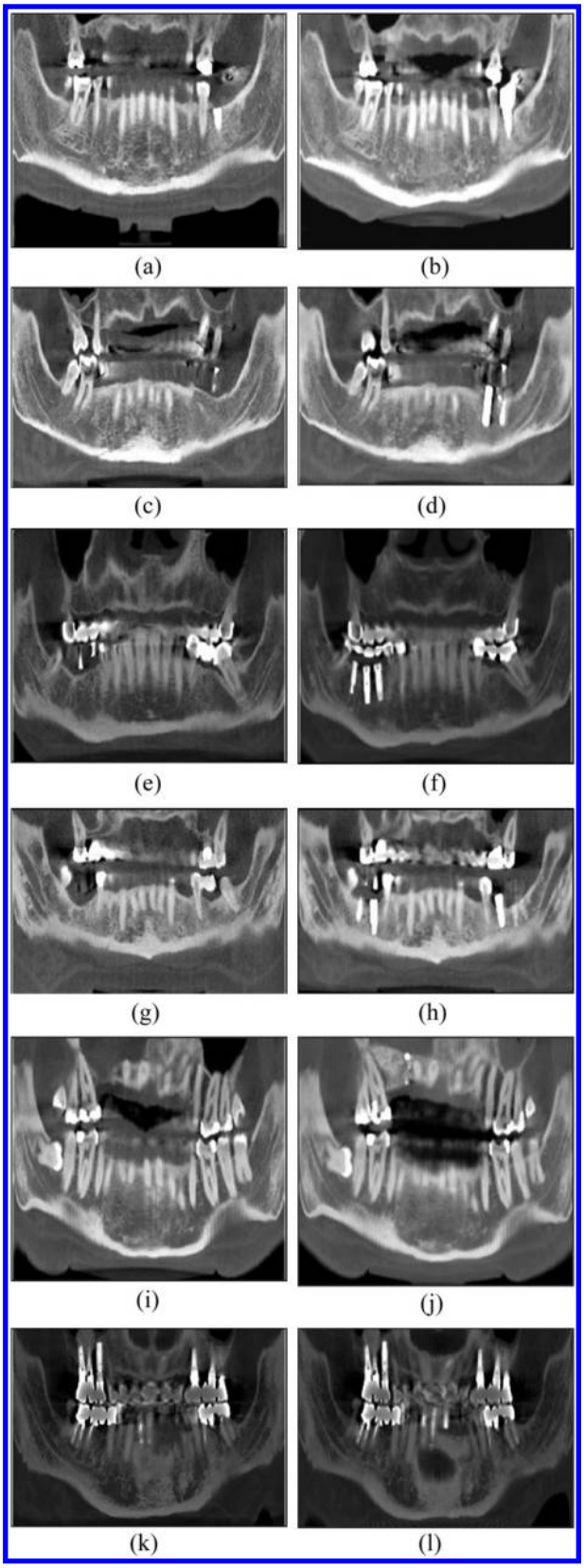

Figure 9 (a–l) The resulting panoramic images of six patients. Each row corresponds to a different patient. The left and right columns represent the pre-operative and post-operative cases, respectively.

operative one. The images presented in Figure 9 have a different width, since their actual width directly depends on the length of the detected dental arch. Further comments and qualitative assessment of the depicted results are provided in the Discussion section.

All panoramic images were reconstructed based on a fitting dental arch which was detected according to the proposed methodology for each examined data set. Table 2 presents the coefficients of the polynomials which approximate the fitting dental arch in each case. Moreover, the corresponding minimum RMSE is also shown for all 34 testing data sets.

Discussion

In this study, a methodological scheme is proposed for automated panoramic image reconstruction from 3D CBCT data. According to the presented methodology, the intensity of each CBCT slice is normalized then converted to a binary image through a standard global binarization algorithm. Next, several morphological filters are applied to extract the curve corresponding to the dental arch. This curve is modelled as a sixth degree polynomial, and it is compared with the template polynomial in terms of the RMSE. All CBCT slices are examined, and the slice corresponding to the minimum RMSE is chosen as the one containing the desired dental arch. Finally, the intensities along the dental arch are projected to produce the panoramic image.

Qualitative evaluation of the results

Typical examples of the produced reconstructed panoramic images are presented in Figure 9. As can be seen in Figure 9, the proposed methodology can successfully represent the information contained in the CBCT data, offering a panoramic view of the maxilla and mandible regions. Moreover, the differences after surgery are also visible, indicating that the proposed technique could be beneficial for the doctor/medical expert when evaluating dental images of a patient acquired at different time intervals.

The saturated (bright) areas of the reconstructed panoramic images correspond to metallic artefacts (implants and fixation screws) which caused the CBCT beam to deflect and thus distorted the original images. However, the proposed methodology is not affected by the aforementioned distortions, as the automatic

Table 2 Polynomial coefficients (in pixels) of the selected fitting dental arch of each case in the testing set and the corresponding minimum root mean square error (min. RMSE, in pixels)

	Polynomial coefficients							
Case	p_0	p_1	p_2	p_3	p_4	p_5	p_6	*Min. RMSE*
#1-pre	2.386	1.597	−7.021	−9.238	55.744	10.159	120.510	22.322
#1-post	9.772	1.776	−38.440	−10.066	103.880	14.051	69.720	18.458
#2-pre	7.681	−2.672	−29.438	13.304	100.020	−3.806	63.934	21.747
#2-post	4.398	−4.134	−14.250	23.438	84.741	−9.746	66.850	23.988
#3-pre	0.7055	2.782	−1.808	−5.782	69.010	2.792	86.306	8.491
#3-post	−2.482	4.656	5.470	−12.236	70.504	3.544	81.452	8.181
#4-pre	16.513	−2.900	−70.636	8.525	148.500	−1.588	54.513	19.107
#4-post	9.195	−5.500	−41.543	25.188	121.690	−8.591	69.163	18.292
#5-pre	21.264	−1.173	−91.732	5.579	181.850	4.788	50.423	14.958
#5-post	17.084	6.550	−77.769	−23.100	158.050	21.009	50.860	23.967
#6-pre	11.933	−3.115	−46.519	12.830	116.560	−3.240	64.341	18.774
#6-post	1.709	−2.344	−8.159	13.683	83.650	−2.945	85.495	13.471
#7-pre	6.452	1.994	−41.886	−7.796	125.620	7.973	50.488	32.984
#7-post	5.845	1.090	−39.826	−3.020	123.960	1.442	57.716	27.074
#8-pre	8.326	10.511	−47.168	−33.642	145.620	23.401	80.719	19.561
#8-post	13.630	−3.375	−49.465	10.627	115.220	−5.071	70.224	12.570
#9-pre	23.815	9.203	−96.678	−25.812	172.960	11.616	68.167	5.120
#9-post	11.900	−2.113	−46.191	2.714	105.000	6.030	93.916	12.241
#10-pre	17.202	−0.798	−65.663	−0.230	137.030	8.241	76.908	7.342
#10-post	5.841	−3.686	−19.832	10.718	83.908	−0.900	88.102	9.240
#11-pre	5.644	0.0697	−30.715	0.490	105.880	−0.971	79.651	7.374
#11-post	4.264	−0.043	−26.466	0.200	103.620	2.333	84.195	6.824
#12-pre	13.800	−2.563	−51.986	6.577	126.650	−6.305	73.331	4.781
#12-post	13.881	−2.875	−49.619	10.157	120.260	−8.942	79.318	5.635
#13-pre	13.998	−10.411	−67.453	37.428	153.280	−26.816	64.823	9.784
#13-post	27.432	−2.550	−102.47	11.177	175.490	−8.698	54.583	11.980
#14-pre	8.651	0.244	−44.476	−0.154	124.170	−1.548	97.507	18.949
#14-post	13.478	4.252	−53.44	−8.792	118.940	5.644	79.729	9.490
#15-pre	10.674	−1.337	−37.102	11.754	88.192	−11.508	110.900	19.586
#15-post	−6.081	−3.880	24.022	18.503	27.648	−15.548	94.719	22.764
#16-pre	−39.837	1.919	99.684	6.262	−5.625	−14.572	102.770	12.942
#16-post	7.421	4.176	−35.891	−13.539	104.540	8.247	82.862	10.756
#17-pre	4.992	−2.961	−24.492	14.351	98.632	−4.582	63.910	23.449
#17-post	0.025	7.934	33.064	−19.907	2.484	8.300	88.738	25.514

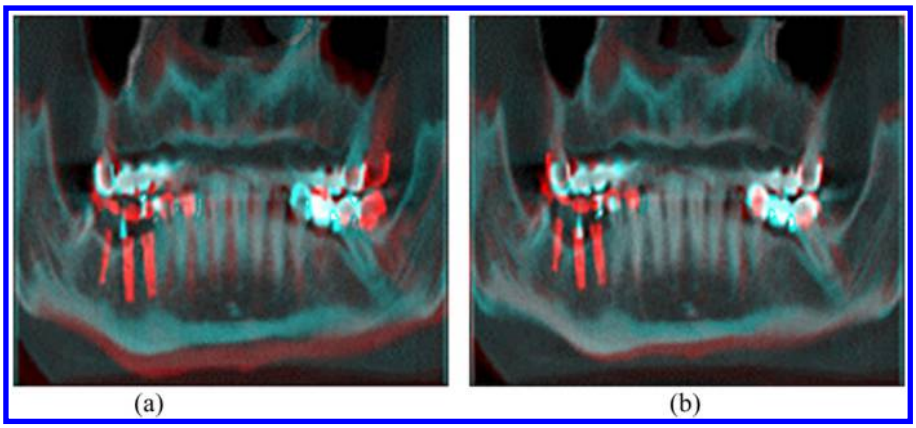

Figure 10 Example of comparing panoramic images reconstructed from (a) misaligned and (b) aligned preoperative and postoperative CBCT volumes. Misalignment errors are visible as ghosting artefacts in lower and right hand side sections of (a) (In the online version a red color tone corresponds to information present only in the postoperative and cyan to information present exclusively in the preoperative panoramic image).

detection of the dental arch and the reconstruction of the panoramic image itself are not hindered. Typical cases are shown in Figure 9g,h and in Figure 9k,l, where metallic artefacts are present. In both cases, good-quality panoramic images were produced.

Image alignment for improved visual assessment

As mentioned, the examination and clinical assessment of the compared pre-operative and post-operative panoramic images can be greatly enhanced if the depicted information is spatially aligned. The alignment of medical imaging data allows the use of digital subtraction radiography techniques which can be utilized to automatically highlight possible differences between the compared images.[14] The usefulness of registration is illustrated in Figure 10, where any differences are annotated using red and cyan tones (red corresponds to information present only in the post-operative and cyan to information present exclusively in the pre-operative panoramic image). In particular, Figure 10a shows the fused pre-operative and post-operative panoramic images produced from misaligned CBCT volumes. As can be seen, there are several ghosting artefacts that render visual assessment quite challenging. On the other hand, Figure 10b presents the panoramic images reproduced from aligned pre-operative and post-operative volumes. In this case, where spurious information caused by spatial deviations is eliminated, the differences resulted from the applied clinical protocol are readily distinguishable.

Control parameters of the proposed methodology

An important parameter of the proposed methodological approach is the value of the threshold used for binarization. The value adopted in this study was automatically calculated from the intensity histograms of the images after intensity normalization. The aim was to find a value that will discard pixels of medium intensity and, at the same time, keep pixels belonging to the dental arch, which have an intensity value close to 1. In particular, an iterative non-linear least squares approach was employed to calculate the mean (μ) and standard deviation (σ) of the Gaussian distribution. A typical intensity histogram is illustrated in Figure 11 where the fitted Gaussian distribution is superimposed. The threshold in the binarization procedure was calculated as $T = \mu + w\sigma$, with $w = 3$.

The weighting parameter w is essential for the automatic calculation of the threshold in the binarization procedure. To make a suitable choice for this parameter,

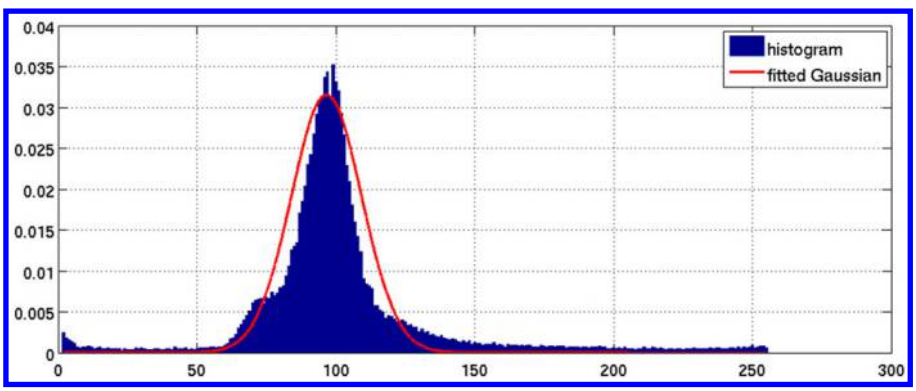

Figure 11 Intensity histogram with Gaussian fitting of the intermediate image obtained after intensity normalization.

three tests were performed, namely the values of $w = 1, 2, 3$ were examined, as it is common practice to consider integer multiples of σ, when working with Gaussian distributions. The respective results are illustrated in Figure 12. There, for each value of w, the results of binarization (left-hand side) and thinning (right-hand side) are presented. As can be seen, values $w = 1$, 2 (Figure 12a–d) do not produce valid results, as the dental arch is not represented by a single curve (due to undesired branching), while $w = 3$ seems to be a more suitable selection for the binarization process.

Another parameter that affects the resulting panoramic images is the radius of the structuring element used for morphological closing. This non-linear procedure is essential for connecting areas between the teeth and for further refining the results of the previous processing step (hole filling). To choose the most suitable value, three tests were performed using structuring elements of radius 5, 11, 15 and 31 pixels, which correspond to radii of 2.0, 4.4, 6.0 and 12.4 mm, respectively. The results are presented in Figure 13.

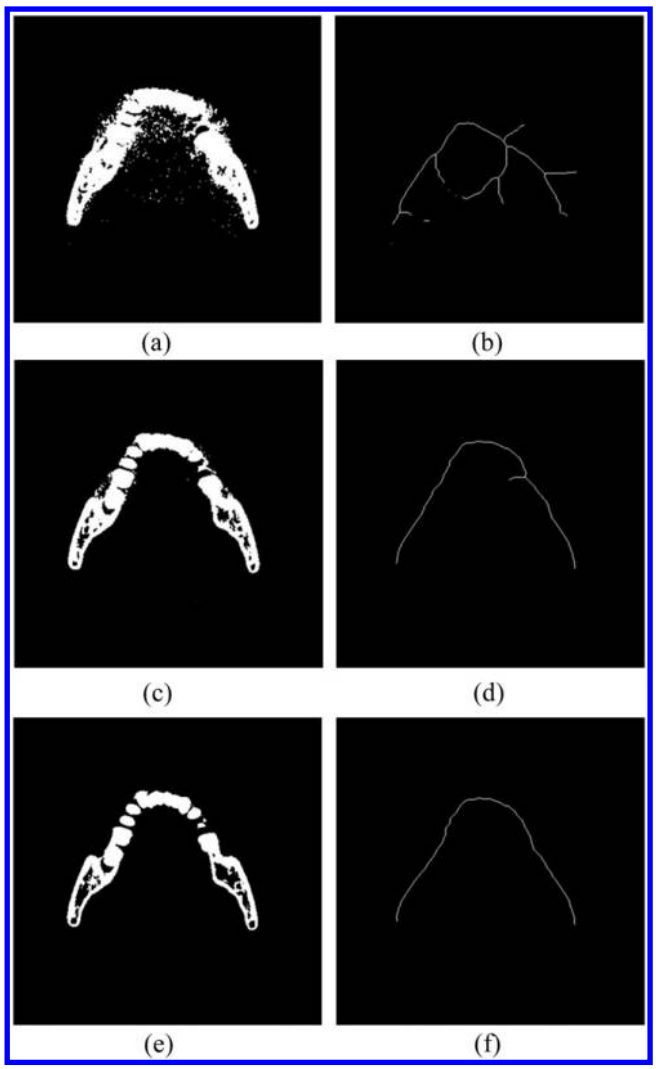

Figure 12 Effect of different values of w in the binarization and thinning process: results of (a) binarization and (b) thinning for $w = 1$, results of (c) binarization and (d) thinning for $w = 2$ and results of (e) binarization and (f) thinning for $w = 3$.

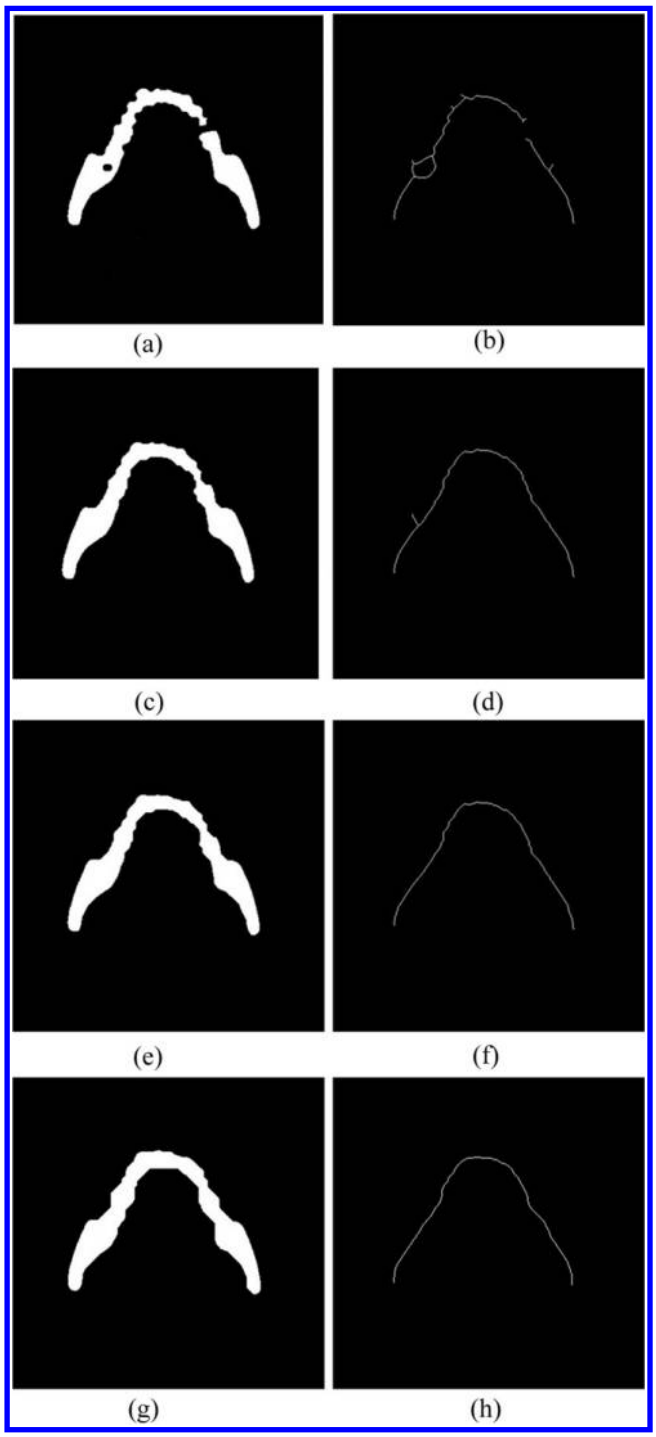

Figure 13 The effect of using different structuring element radii in the closing and thinning process: results of (a) closing and (b) thinning for a radius of 5 pixels, results of (c) closing and (d) thinning for a radius of 11 pixels, results of (e) closing and (f) thinning for a radius of 15 pixels and results of (g) closing and (h) thinning for a radius of 31 pixels.

Table 3 Root mean square error values (in pixels) for each examined polynomial degree, for all subjects in the training set

	Polynomial degree				
Subject	*Second*	*Third*	*Fourth*	*Fifth*	*Sixth*
#1	10.880	10.817	7.252	7.127	4.850
#2	6.934	6.909	6.097	6.098	3.564
#3	7.466	6.594	3.874	3.828	2.990
#4	6.753	6.751	4.538	4.538	2.508
#5	7.872	7.860	4.557	4.558	3.556
#6	6.875	6.691	3.692	3.618	2.963
#7	10.062	9.779	4.675	4.644	3.491
#8	9.338	9.241	4.800	4.798	2.486
$\mu \pm \sigma$	8.273 ± 1.604	8.080 ± 1.650	4.936 ± 1.182	4.901 ± 1.166	3.301 ± 0.763

Specifically, Figure 13a,b presents the result of morphological closing and thinning operation, using a structuring element with a radius of 5 pixels. As can be seen, the results are not valid since the dental arch is separated into two regions and thus is non-continuous. In addition, Figure 13c,d illustrates the case where a structuring element with a radius of 11 pixels is used. In this case, the dental arch is a unified, continuous region; however, an undesirable spike is present after thinning (Figure 13d). In Figure 13e,f, the case of utilizing a structuring element with a radius of 15 pixels is presented. In this case, the detection of the dental arch is successful, without any spikes or non-continuous regions. Finally, an extreme radius value of 31 pixels was also considered (Figure 13g, h), but no noticeable difference is observed, hence a radius value of 15 pixels was preferred.

Selection of template polynomial degree

As mentioned, arch detection is based on the comparison with the template polynomial, which is obtained using the training set. The most important part of constructing the template polynomial is to define its degree. For this reason, polynomials of several degrees were examined, and for each one of them, a measure of the degree of fit was employed.[21] In particular, a standard RMSE metric [Equation (4)] was used to evaluate how well the fitness is performed for each polynomial degree.

For each one of the eight manually chosen training data sets, five fitting procedures were performed, corresponding to polynomial degrees of 2, 3, 4, 5 and 6, respectively. The results of those procedures are illustrated in Table 3. Specifically, each row corresponds to each examined case included in the training set and each column corresponds to a polynomial degree. As can be seen in Table 3, for every case the RMSE value decreases as the polynomial degree increases. This is also reflected in the mean RMSE value of each polynomial degree shown in the last row. From these measurements a polynomial of degree 6 seems to be a suitable choice. Polynomials of greater degrees were examined but not considered as such polynomials may well cause the inclusion of undesired outlier data points in the model, which would hinder the overall form quality of the modelled arch.

Multiple dental archs

Another aspect concerning the panoramic image reconstruction is the total number of dental arch curves which are utilized. In particular, it is possible to use additional dental arch curves which could be obtained by computing parallel offsets of the initially detected curve. An example of such a case is illustrated in Figure 14, where the central (red) curve represents the initial dental arch (as shown in Figure 6) with its parallel offsets of 2, 4 and 6 pixels respectively (green, yellow and blue). Each one of these offset curves creates a different panoramic image. A combined panoramic image can then be reconstructed by considering the average intensity of all offset panoramic images.

To examine whether the introduction of additional offset panoramic images could enhance the final result, an error metric was calculated. The panoramic image derived from a single curve was compared with the panoramic image obtained from three, five and seven curves in terms of the intensity root mean square error (IRMSE), as shown below:

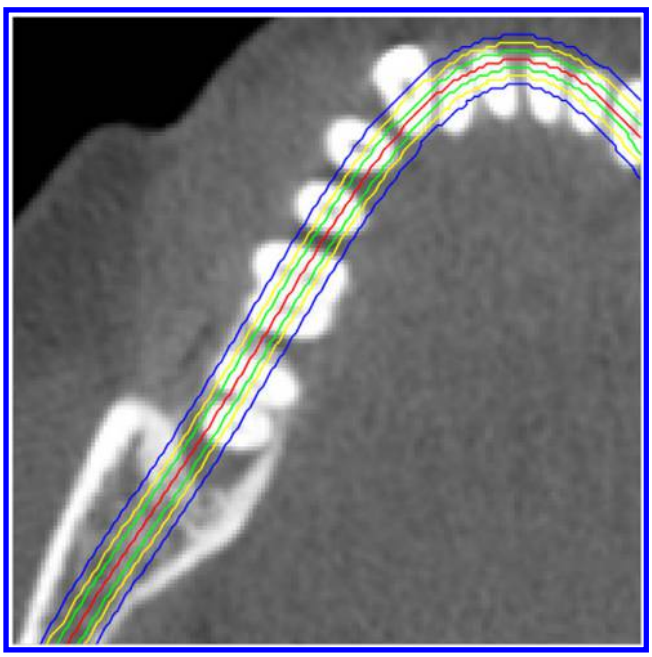

Figure 14 Initial dental arch (central curve) and its parallel offsets of 2, 4 and 6 pixels.

$$\mathrm{IRMSE}=\sqrt{\frac{1}{N\times M}\sum_{i=1}^{N}\sum_{j=1}^{M}[I_1(i,j)-I_k(i,j)]^2} \qquad (5)$$

where N, M are the image's dimensions, I_1 and I_k are the panoramic images calculated using the initial dental arch curve and the kth parallel curve, respectively.

All these IRMSE values were calculated for all subjects in the testing set, for both pre-operative and post-operative cases. The calculated IRMSE values between the images produced using one, three, five and seven curves were insignificant (in the order of 10^{-3}). In particular, the average IRMSE values between the one and three curve cases were 2.36×10^{-3} and 2.59×10^{-3} for pre-operative and post-operative data, respectively. Likewise, the average IRMSE values between one and five curves were 3.95×10^{-3} and 4.35×10^{-3}. Finally, the average IRMSE values between one and seven curves were 6.6×10^{-3} and 7.43×10^{-3}. Therefore, additional parallel curves do not contribute to the accuracy of the final result and hence a single curve implementation was preferred in this study.

Application limitations

The proposed methodology is based on the selection of a suitable training set, which should include the most characteristic and ideally formed dental arches from the examined data, leading to the calculation of accurate polynomial models. It follows that the selected training data sets can only be used for cases of data acquired using similar acquisition parameters. In case the data acquisition parameters change, which would lead to the generation of different imaging data, then a new training data set, better describing the particular data, would have to be utilized instead. Nevertheless, since this is rarely the case in a clinical environment, as specific, fixed acquisition parameters are used for certain conditions or medical procedures, a single training data set would usually suffice in most cases.

Conclusion

In this study, an automated methodology is proposed for panoramic image reconstruction from 3D CBCT data, which is independent of the utilized hardware. In particular, from the initial data set consisting of 21 data pairs (pre-operative and post-operative cases), 8 data sets were selected to calculate the dental arch's template polynomial. The rest of the data sets (34) were used as testing data. All slices of each data set were processed according to the proposed methodology, and the RMSE value between the extracted and the template polynomial was calculated. The dental arch corresponding to the minimum RMSE was considered to calculate the panoramic image through intensity projection. The proposed study showed the feasibility of reconstructing panoramic dental images from already acquired CBCT scans, through a fully automated procedure. Therefore, provided that the CBCT scans are available, there is no need for an additional invasive procedure to acquire the desired panoramic images. The proposed methodology performed consistently in all examined cases and was not negatively affected by metallic artefacts which cause extensive distortion to radiographic images. Moreover, the synthesized panoramic images can be readily used for evaluative purposes.

Acknowledgments

The authors thank Dr Peter Windisch and his team at the Department of Periodontology, Semmelweis University, Budapest, Hungary, for providing us with the necessary data sets for conducting this study.

References

1. White SC, Pharoh MJ. *Oral Radiology and Interpretation*. St Louis, MO: Mosby; 2005.
2. Whaites E. *Essentials of dental radiography and radiology*. 4th edn. Edinburgh, UK: Churchill Livingstone; 2007. pp. 187–206.
3. Farman AG, Farman TT. Extraoral and panoramic systems. *Dent Clin North Am* 2000; **44**: 257–72, v–vi.
4. Akarslan ZZ, Akdevelioğlu M, Güngör K, Erten H. A comparison of the diagnostic accuracy of bitewing, periapical, unfiltered and filtered digital panoramic images for approximal caries detection in posterior teeth. *Dentomaxillofac Radiol* 2008; **37**: 458–63. doi: https://doi.org/10.1259/dmfr/84698143
5. Thali MJ, Markwalder T, Jackowski C, Sonnenschein M, Dirnhofer R. Dental CT imaging as a screening tool for dental profiling: advantages and limitations. *J Forensic Sci* 2006; **51**: 113–9. doi: https://doi.org/10.1111/j.1556-4029.2005.00019.x
6. GE Healthcare, Dentascan, Accessed (cited) 31 January 2017, Available from: http://www3.gehealthcare.com/en/products/categories/advanced_visualization/applications/dentascan
7. Chanwimaluang T, Sotthivirat S, Sinthupinyo W. Automated dental arch detection using computed tomography images. Proceedings of the 9th International Conference on Signal Processing; 2008. pp. 737–40.
8. Han B, Chen L, Cai S, Pu X, Fang LD, Li S, et al. An automatic method of synthesizing panoramic radiograph by unwrapping dental CT image. International Conference on Mechatronic Science, Electric Engineering and Computer; 2011. pp. 1094–6.
9. Saing V, Wangkaoom K, Thongvigitmanee S. Automatic dental arch detection and panoramic image synthesis from CT images. 35th Annual International Conference of the IEEE EMBS. Osaka, Japan; 3–7 July 2013. pp. 6099–102.
10. Akhoondali H, Zoroofi RA, Shirani G. Fully automatic extraction of panoramic dental images from CT-scan volumetric data of the head. *J Appl Sci* 2009; **9**: 2106–14. doi: https://doi.org/10.3923/jas.2009.2106.2114
11. Pal NR, Pal SK. Entropic thresholding. *Signal Process* 1989; **16**: 97–108. doi: https://doi.org/10.1016/0165-1684(89)90090-X
12. SkyView 3D CBCT. Updated Accessed (cited) 29 February 2016. Available from: http://my-ray.co.uk/skyview-3d-cbct/
13. GE Healthcare, Dentascan, Accessed (cited) 31 January 2017, Available from: http://www.i-cat.com/products/i-cat-for-orthodontics/
14. Economopoulos TL, Asvestas PA, Matsopoulos GK, Molnár B, Windisch P. Volumetric difference evaluation of registered three-dimensional pre-operative and post-operative CT dental data. *Dentomaxillofac Radiol* 2012; **41**: 328–39. doi: https://doi.org/10.1259/dmfr/94040044
15. Soille P. *Morphological image analysis: principles and applications*: Springer-Verlag; 1999. pp. 173–4.

16. Vincent L. Morphological grayscale reconstruction in image analysis: applications and efficient algorithms. *IEEE Trans Image Process* **2**; 1993: 176–201. doi: https://doi.org/10.1109/83.217222
17. Gonzalez RC, Woods RE, Eddins SL. *Digital image processing using MATLAB*. 2nd edn: Gatesmark Publishing; 2009.
18. Dougherty ER. *An introduction to morphological image processing*. Bellingham, WA: SPIE Optical Engineering Press; 1992.
19. Lam L, Lee SW, Suen CY. Thinning methodologies—a comprehensive survey. *IEEE Trans Pattern Anal Mach Intell* **14**; 1992: 869–85. doi: https://doi.org/10.1109/34.161346
20. MATLAB Image Processing Toolbox, Accessed (cited) 31 January 2017, Available from: https://www.mathworks.com/products/image/
21. Glover DM, Jenkins WJ, Doney SC. Least squares and regression techniques, goodness of fit and tests, non-linear least squares techniques. Woods Hole Oceanographic Institute; 8 July 2008.

Appendix A

Hole filling

To implement the hole-filling algorithm, it is essential to define a marker image as shown in the following equation:

$$Y(i,j)=\begin{cases} 1-I_B(i,j), & \text{if (i,j) is on the border of } I_B \\ 0 & \text{otherwise} \end{cases} \quad \text{(A1)}$$

where I_B^c is the complement of the binary image I_B and $Y(Y \subseteq I_B^c)$ the marker image.

Next, the reconstruction of the image I_B^c from Y is obtained through an iterative procedure of elementary dilations of Y inside I_B^c until convergence is achieved. This operation is illustrated in the following equation:

$$\rho_{I_B^c}(Y)=\bigcup_{n\geq 1}\delta_{I_B^c}^{(n)}(Y) \quad \text{(A2)}$$

with $\delta_{I_B^c}^{(1)}(Y)=(Y\oplus E_1)\cap I_B^c$, where E_1 is a 3×3 structuring element featuring eight-connectivity, $\oplus$ is the dilation operator and n is the number of iterations.

This iterative procedure stops when two subsequent iterations produce the same result, *i.e.* $\delta_{I_B^c}^{(n+1)}(Y)=\delta_{I_B^c}^{(n)}(Y)$. The final image with all holes filled (I_F) is obtained by complementing the result of Equation (A3), as shown below:

$$I_F=\left[\rho_{I_B^c}(Y)\right]^c \quad \text{(A3)}$$

Morphological closing

Morphological closing can be performed by applying the following equation:

$$I_{close}=(I_F\oplus E_2)\ominus E_2 \quad \text{(A4)}$$

where E_2 is a disc-shaped structuring element with a radius of 15 pixels and $\ominus$ is the erosion operator.

Morphological thinning

Thinning is expressed as shown in the following equation:

$$I_{thin}=I_{close}\otimes E_3=I_{close}\backslash(I_{close}\odot E_3) \quad \text{(A5)}$$

where \ denotes the set difference operation, $\odot$ expresses the hit–miss transform and E_3 is a 3×3 structuring element.

The algorithm employed in this study is based on some well-defined conditions for discarding an examined pixel p. Those conditions are summarized below:

(a) $\sum_{i=1}^{4} b_i=1$

$$b_i=\begin{cases} 1, & x_{2i-1}=0\wedge(x_{2i}=1\vee x_{2i+1}=1) \\ 0, & \text{otherwise} \end{cases}$$

considering the following neighbourhood ordering:

x_4	x_3	x_2
x_5	p	x_1
x_6	x_7	x_8

(b) $2\leq \min\{\sum_{i=1}^{4} x_{2i-1}\vee x_{2i}, \sum_{i=1}^{4} x_{2i}\wedge x_{2i+1}\}\leq 3$

(c) $(x_2\vee x_3\vee \bar{x}_8)\wedge x_1=0$

(d) $(x_6\vee x_7\vee \bar{x}_4)\wedge x_5=0$

where $\vee$ and $\wedge$ express the logical "OR" and "AND" operations, respectively, and $\bar{x}$ is the pixel's complement.

To discard an examined pixel p, two sets of conditions should be satisfied in each iteration of the algorithm. Firstly, conditions (a), (b) and (c) must be satisfied, and secondly, conditions (a), (b) and (d) must apply in order for a pixel p to be deleted. In the current implementation, this procedure was performed until the image no longer changed, *i.e.* the total number of iterations was not defined beforehand.